Article

Qualitative Comparison of Lock-in Thermography (LIT) and Pulse Phase Thermography (PPT) in Mid-Wave and Long-Wave Infrared for the Inspection of Paintings

Michaël Hillen [1,*], Seppe Sels [1], Bart Ribbens [1], Simon Verspeek [1], Koen Janssens [2], Geert Van der Snickt [2,3] and Gunther Steenackers [1]

[1] InViLab, University of Antwerp, Groenenborgerlaan 171, B-2020 Antwerp, Belgium
[2] AXIS, University of Antwerp, Groenenborgerlaan 171, B-2020 Antwerp, Belgium
[3] ARCHES, University of Antwerp, Mutsaardstraat 31, B-2000 Antwerp, Belgium
[*] Correspondence: michael.hillen@uantwerpen.be

Abstract: When studying paintings with active infrared thermography (IRT), minimizing the temperature fluctuations and thermal shock during a measurement becomes important. Under these conditions, it might be beneficial to use lock-in thermography instead of the conventionally used pulse thermography (PT). This study compared the observations made with lock-in thermography (LIT) and pulse phase thermography (PPT) with halogen light excitation. Three distinctly different paintings were examined. The LIT measurements caused smaller temperature fluctuations and, overall, the phase images appeared to have a higher contrast and less noise. However, in the PPT phase images, the upper paint layer was less visible, an aspect which is of particular interest when trying to observe subsurface defects or the structure of the support. The influence of the spectral range of the cameras on the results was also investigated. All measurements were taken with a mid-wave infrared (MWIR) and long wave infrared (LWIR) camera. The results show that there is a significant number of direct reflection artifacts, caused by the use of the halogen light sources when using the MWIR camera. Adding a long-pass filter to the MWIR camera eliminated most of these artifacts. All results are presented in a side-by-side comparison.

Keywords: non-destructive testing; infrared thermography; cultural heritage; paintings

1. Introduction

Active infrared thermography (IRT) can be employed to document differences in the structure and material composition of objects. During IRT, an object is thermally excited and the thermal response of the object is measured, on the surface, by an infrared camera. Two main types of IRT are pulse thermography (PT), which is relatively straightforward and easy to use, where the object is thermally excited by a short rectangular pulse and then returns to an equilibrium, and lock-in thermography (LIT), where the object is subjected to continuous thermal excitation by a periodic signal. LIT has a potentially higher signal-to-noise ratio than PT [1,2], which would mean it could achieve comparable or better results at lower temperature fluctuations. It also allows for a more gradual heating up of the object, reducing thermal shocks [2]. This is of particular interest when inspecting cultural heritage objects, where temperature fluctuations must be minimized in order to prevent degradation. In preventive conservation, often a fluctuation of $\pm 3\,^{\circ}C$ per 24 h is suggested as a threshold value.

Because IRT is a contactless and non-destructive technique that can easily be used in situ, it is of interest to conservators. It is, therefore, becoming more widely adopted in heritage science, a field that recently reported various advances in the development of different imaging modalities [3]. Thus far, the applicability of IRT has been explored to inspect a variety of cultural heritage objects. The studied objects include, but are not limited

to, paintings [2,4–12], frescoes [13–15], mosaics [14,16,17], marquetries [7,18,19], ancient texts [1,6,20], ancient bronzes [1,6,20], glass-in-lead windows [15,21,22] and ceramics [15]. Specifically, for paintings, IRT has successfully been employed to detect several kinds of defects [2,4,6,8–12,23] and hidden compositions [4–7], as well as to visualize the woodgrain in panel paintings [4,5,7,9,10] and the weave pattern of the canvas [5,7–9]. For these purposes, several well-known PT processing methods are employed, such as Principal Component Thermography (PCT) [4,5,7–9], Partial Least Squares Thermography (PLST) [8], Pulse Phase Thermography (PPT) [6,9,11], Differential Absolute Contrast (DAC) [10] and Thermal Signal Reconstruction (TSR) [12]. The advantages and disadvantages of the most prominently used methods have been discussed by Gavrilov et al. [23] and Meav et al. [9].

In contrast, LIT was tested to a much lesser extent [2,7]. Recently, a novel technique called pulse-compression thermography has also been used [2], which also shows promise as a way to minimize heat fluctuations during measurements.

Thermal cameras generally operate in the mid-wave infrared (MWIR) spectral range (3–5 μm) or the long-wave infrared (LWIR) spectral range (7–14 μm). An added value of MWIR cameras is that they can also be used for infrared reflectography (IRR) measurements [6,7,13,24], a routine imaging technique in the museum field, which provides complementary information. In this way, an MWIR camera setup could allow for performing both measurements with the same system, which simplifies image registration between the different imaging modalities.

As discussed, there already exist a variety of studies where IRT is used for the evaluation of cultural heritage objects. In these studies, various cameras that operate in different wavelength ranges are used, but the effect of the selected wavelength range on the results is almost never considered [7,25]. LIT could potentially operate with lower temperature fluctuations than PT, but these techniques have not been compared for the inspection of paintings.

In this study, the performance of LIT was compared with that of PPT, a prominently used PT technique that is closely related to LIT. In order to investigate the influence of the spectral range of the camera, measurements were taken with both MWIR and LWIR cameras. All the measurements were performed on three paintings with different compositions. The results are presented as a side-by-side comparison, so a reader can easily assess the differences.

2. Materials and Methods

2.1. Test Sample Description

In order to compare the observations made with the different instruments and techniques, three paintings with differing materials and compositions were examined. The first is a 19th century Russian icon that depicts Saint Nicholas of Myra (Figure 1a), painted on a wooden panel of 14 cm × 18 cm. The painting's surface shows various small surface defects and, previous IRR demonstrated the presence of an underlying preparatory underdrawing in pencil. For reference, this painting has also been investigated using Macroscopic Fourier Transform Infrared scanning in Reflection mode (MA-rFTIR) [26] and PT [7].

A portrait of unknown origin, painted in the style of Rembrandt on a wooden panel of 18 cm × 21 cm (Figure 1b), was also examined. This portrait is considered to be a reduced-size copy of a self-portrait of Rembrandt of 1633, now in the collection of the Louvre Museum, Paris (inv. 1745). In contrast to many original works by Rembrandt, where often a thick (impasto) paint is employed in the lighter tones, this copy is very thinly painted.

The third work is a 20th century icon painting depicting St. George slaying the dragon on a gilded background (Figure 1c). It was painted on canvas that was glued on to a wooden panel with a fixed frame, measuring 35 cm × 42 cm in total. The painted surface is heavily cracked, and there are large paint lacunae where the canvas is exposed in several locations.

Figure 1. (**a**) RGB image of the 19th century Russian icon showing St. Nicholas (14 cm × 18 cm). The paint's surface shows various small surface defects and there is a preparatory sketch in pencil beneath the painted surface. (**b**) RGB image of a reduced-size copy of an auto-portrait by Rembrandt (18 cm × 21 cm), with the frame removed. (**c**) RGB image of the St. George painting (35 cm × 42 cm). The surface shows several large paint lacunae, exposing the canvas substrate that was glued onto the panel.

2.2. Setup and Instrumentation

The paintings were thermally excited by two 2 kW EDEVIS halogen lamps. These lamps are covered by a double glass plate, which helps reduce the IR emissions from the lamps. Halogen lamps can be used for both LIT and PPT measurements, since the emitted intensity can easily be controlled by adjusting the voltage, and they are convenient to use in situ. In these experiments, the intensity of the lamps was adjusted with a 0–10 V controller. The lamps were positioned at 1 m distance to the painting, at a 60° angle to the surface. The distance between the camera and artwork was adjusted so the entire artwork fitted into the camera frame. A detailed schematic of the setup is shown in Figure 2.

Two different cameras, one with a spectral response in the MWIR range and one in the LWIR range, and a total of three distinct camera setups were used to measure the paintings. The first setup used a FLIR X6540sc actively cooled thermal camera. This camera is sensitive in the 1.5–5.5 µm spectral range, has a Noise Equivalent Temperature Difference (NETD) of <25 mK (typically 18 mK), which is the minimum temperature difference a thermal camera can resolve, and a 640 × 512 pixel resolution. An L1009 25 mm lens was used, which has a spectral range of 2.5–5 µm and an Angular Field Of View (AFOV) of 22° × 17°. This setup, referred to as "A-MWIR_O", has a large amount of overlap with the emission spectrum of the halogen lamps. The second setup, referred to as "B-MWIR_F", used the same camera, with a long-pass filter, which was used to block most of the light emitted by the halogen lamps. The cut-on wavelength of this filter is 4.1 µm. The final setup, referred to as "C-LWIR", used a FLIR A655sc thermal camera. This camera is sensitive in the 7.5–14.0 µm spectral range, has an NETD of <30 mk and a 640 × 480 pixel resolution. A 24.6 mm lens was used, which has an AFOV of 25° × 19°. Table 1 shows a summary of the three camera setups and their most important characteristics. All measurements were performed at a 50 Hz framerate, which is the locked framerate of the A655sc camera, in order to eliminate the influence of the framerate on the results. Using a higher framerate would increase the amount of frames for a certain time period, which reduces the noise in the processed images.
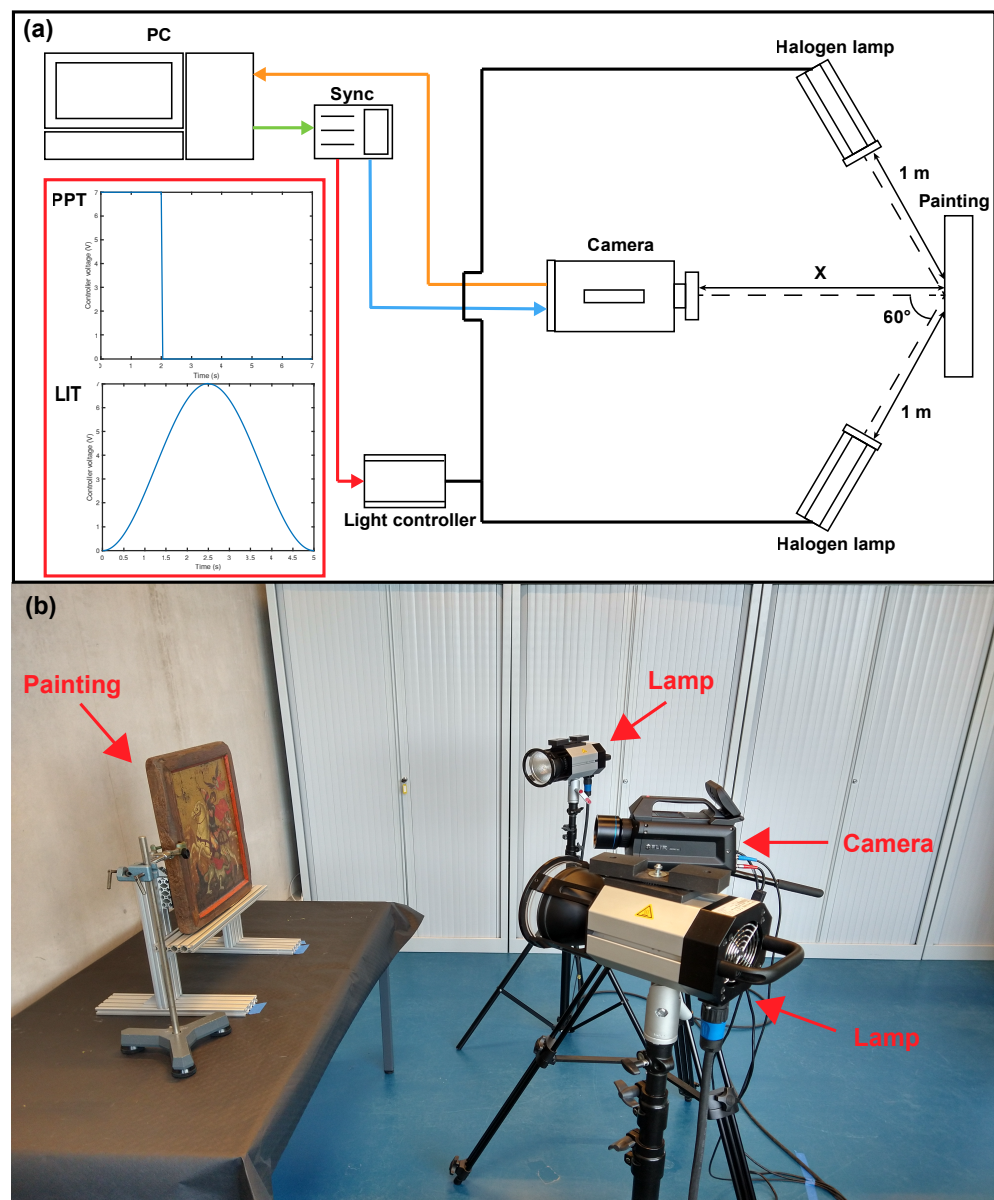
Figure 2. (**a**) Schematic of the measurement setup. Either a short pulse (PPT) or a modulated sinusoidal wave (LIT) is sent to the light controller. The distance between the painting and the camera depends on the size of the painting. (**b**) RGB image showing the measurement setup during experiments, on the Saint-George icon.

Table 1. Summary of the used camera setups and their most important characteristics.

Name	Model	Spectral Range (μm)	NETD (mK)
A-MWIR _O	FLIR X6540sc	2.5–5.0	<25
B-MWIR _F	FLIR X6540sc	4.1–5.0	<25
C-LWIR	FLIR A655sc	7.5–14.0	<30

2.3. Measurement and Processing

In LIT [27], the object is submitted to a frequency-modulated, sinusoidal thermal excitation. In the stationary regime, the thermal response of the object to this excitation is also sinusoidal, with a phase and amplitude that depends on the characteristics of the input wave. Higher modulation frequencies confine the thermal response to the surface of the object, while lower frequencies have a deeper depth range [28]. The minimum measurement

duration is one full period, but ideally the measurement lasts multiple modulation cycles, until the object reaches a stationary regime [27].

The paintings were measured at a modulation frequency of 0.2 Hz and an amplitude of approximately 1.4 kW lamp power per lamp. Decreasing the frequency further did not seem to reveal additional information, and eventually led to blurry images because of increased lateral heat transfer. The paintings were measured for only one full heating period, in order to limit the heating up of the painting as much as possible. The maximum temperature fluctuation during the measurement was 1.8 °C. The signal that was used to control the lamps is shown in Figure 2, while Figure 3 shows the pixel intensity fluctuation during the measurement. The intensity plot clearly indicates that the thermal response of the object is not entirely sinusoidal. There is also a slight delay between the lamps receiving the signal and the object heating up.
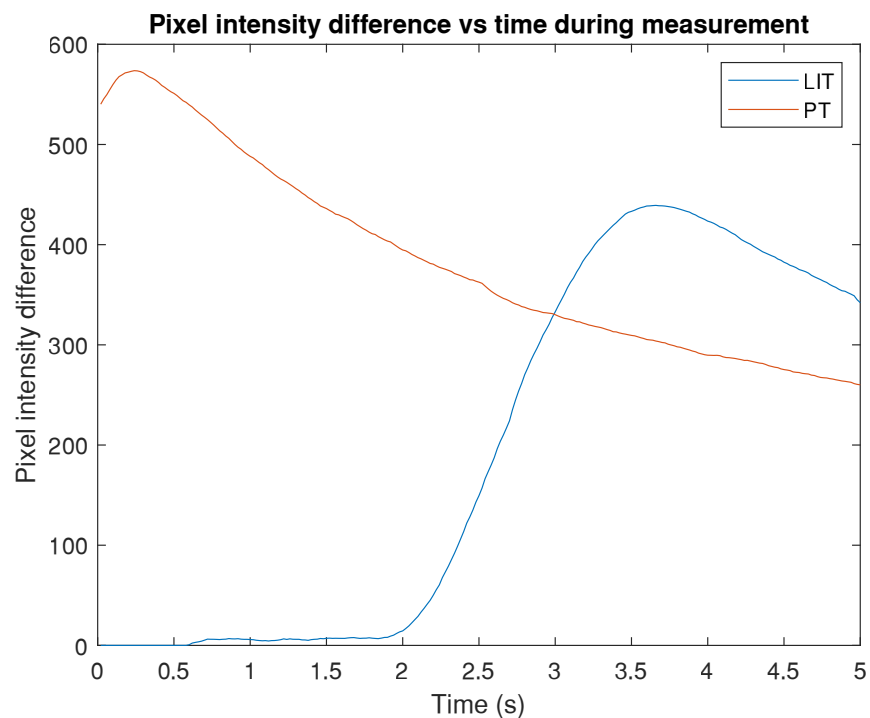
Figure 3. Pixel intensity evolution during a measurement. For the LIT measurement, the entire measurement cycle is shown. For the PT measurement, the cool-down process is shown.

Phase and amplitude images can be derived from just four thermograms, located equidistantly on the sinusoidal modulation cycle [27,28]. However, because of the very limited amount of data points, this method produces noisy images. An alternative processing method was used [27,29], where the entire measured image sequence was multiplied by two reference functions of known phases, differing by 90°, and the products were then added, in order to produce the in-phase and out-of-phase components for each pixel:

$$0° = \sum_t \sin(2\pi\omega t + \frac{3\pi}{2}) * T(t), \tag{1}$$

$$90° = \sum_t \cos(2\pi\omega t + \frac{3\pi}{2}) * T(t). \tag{2}$$

where ω is the modulation frequency and $T(t)$ is the measured thermal response at a specific time. Both reference functions are phase-shifted by $\frac{3\pi}{4}$, so the in-phase component has the

same phase-shift as the sinusoidal wave that is used for thermal excitation. The amplitude and phase components for each pixel can then be calculated as follows:

$$A = \sqrt{(0°)^2 + (90°)^2},$$ (3)

$$\phi = \tan^{-1}(\frac{90°}{0°}).$$ (4)

In PPT [28,30–32], the object is thermally excited by a rectangular pulse, varying from several milliseconds to a few seconds, depending on the thermal properties of the object under inspection. When an object undergoes pulse excitation, thermal waves of various phases and amplitudes simultaneously excite the object in a transient regime. This is in contrast with LIT, where the object is excited by a single frequency and amplitude in a stationary regime. PTT is able to probe multiple depths in one measurement, while LIT requires a separate measurement for each depth [28].

Each of the three paintings were thermally excited by a 2 s rectangular pulse at approximately 1.4 kW lamp power per lamp. The maximum temperature fluctuation during the measurement was 2.7 °C. The subsequent cool-down process was captured for 5 s. Increasing the cool-down time reduced the noise in the processed images but also made them blurrier. The signal that was used to control the lamps is shown in Figure 2, while Figure 3 shows the pixel intensity fluctuation during the cool-down process.

The frequencies for each pixel of the PPT measurement can be extracted from the cool-down sequence by using the discrete Fourier transform:

$$F_n = \sum_{k=0}^{N-1} T(k)e^{\frac{2\pi i k n}{N}} = Re_n + iIm_n.$$ (5)

where $T(k)$ is the measured thermal response of frame k, and Re_n and Im_n are the real and imaginary parts of the transform, and subscript n designates the frequency increment. The amplitude and phase components for each pixel and frequency increment can then be calculated with:

$$A_n = \sqrt{Re_n^2 + Im_n^2},$$ (6)

$$\phi_n = \tan^{-1}(\frac{Re_n}{Im_n}).$$ (7)

This results in a stack of n phases and a second stack of n amplitude images, where lower frequencies can penetrate deeper into the object. In our experience, only the lower frequency phase images are usable, while the others mainly contain noise. For the purpose of comparison, the images at the lowest frequency, 0.2 Hz, were selected, which is also the modulation frequency used for the LIT measurements.

Both the LIT and the PPT methods produce amplitude and phase images. Phase images are less influenced by heating and optical non-uniformities, and their depth penetration is about twice the depth penetration of amplitude images [30]. However, phase images are affected more by noise than amplitude images, especially at high frequencies [32].

3. Results and Discussion

For the A-MWIR_O camera setup there was a substantial overlap between the emission spectrum of the halogen lamps and the spectral range of the sensor. As a result, reflections of the primary radiation of the halogen lamps by the object caused direct reflection artifacts during the measurement. LIT measurements were affected the most, since the lamps were turned on for almost the entire duration of the measurement. Nevertheless, the PPT measurements were significantly hampered by these artifacts as well, which were caused by infrared radiation being emitted by the lamps even after they were turned off. The effect of these artifacts was most noticeable for the measurements of the St George painting,

with the surface composition being clearly distinguishable, even in the phase images (Figure 4). This type of artifact is a known issue that is covered in the literature [33,34]. The measurements of the other artworks were also affected by these artifacts, but to a lesser degree (Figures 5 and 6). Adding a long-pass filter with a cut-on wavelength of 4.1 μm to the MWIR camera (setup B-MWIR_F) eliminated most, if not all, direct-reflection artifacts.

After these artifacts had been eliminated, the spectral range of the sensor did not seem to have much of an impact. As shown by Figures 4–6, the phase images for the measurements taken with B-MWIR_F and C-LWIR all look very similar to each other. However, B-MWIR_F phase images had a slightly better contrast compared to C-LWIR ones, which resulted in a more pronounced visualization of the wooden support structure (Figure 5). This was likely caused by the lower NETD of B-MWIR_F compared to C-LWIR.

In the phase images of the Rembrandt copy, the upper paint layer became almost entirely invisible and the structure of the wooden board below was revealed (Figure 5). For the purpose of visualizing the wooden structure of the board, PPT seemed to be preferable to LIT, since less of the upper paint layer remained visible in the PPT phase images. On the other hand, the lines of the pencil drawings of the painted icon and other small surface defects appeared to have a higher contrast in the phase image of the LIT measurement (Figure 6). Overall, the LIT images appeared to have a higher contrast, and appeared to be less noisy, when compared to the PPT images.
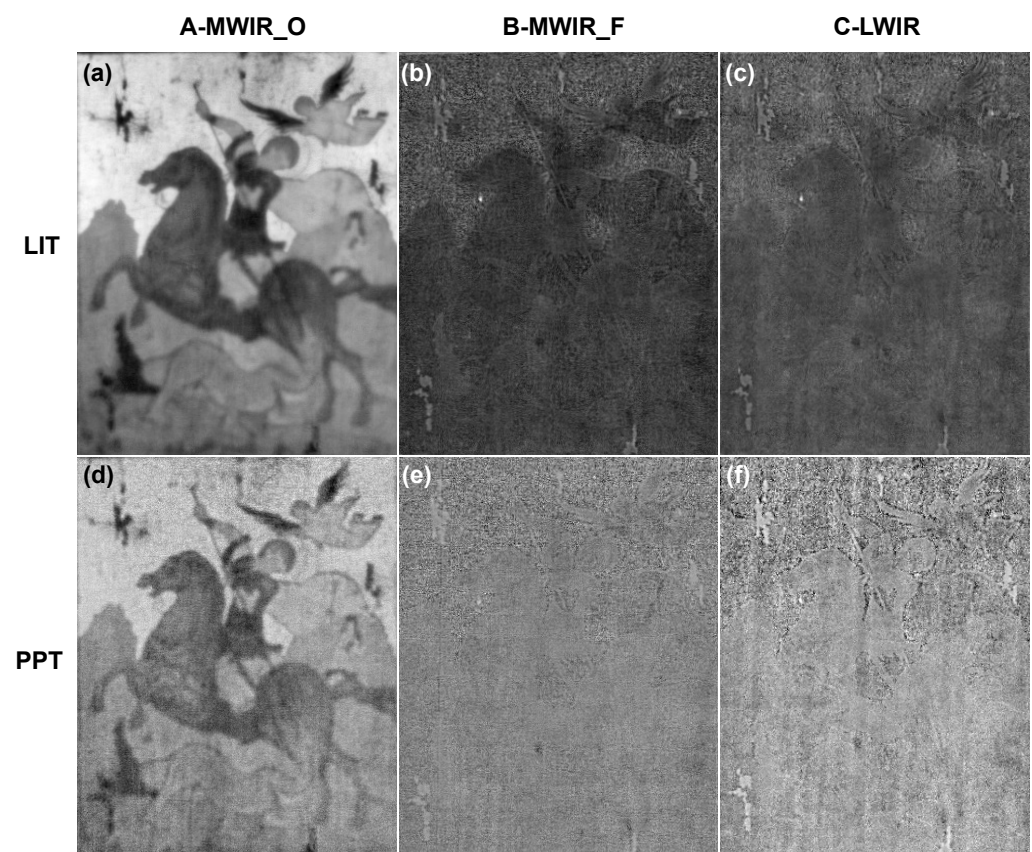
Figure 4. LIT and PPT phase images of the St George painting for all camera setups. Both LIT and PPT measurements were heavily influenced by reflections from the halogen lamps (**a**,**d**). The influence of these reflections was eliminated when using a long-pass filter (**b**,**e**) and the results look very similar to those of the LWIR camera (**c**,**f**).
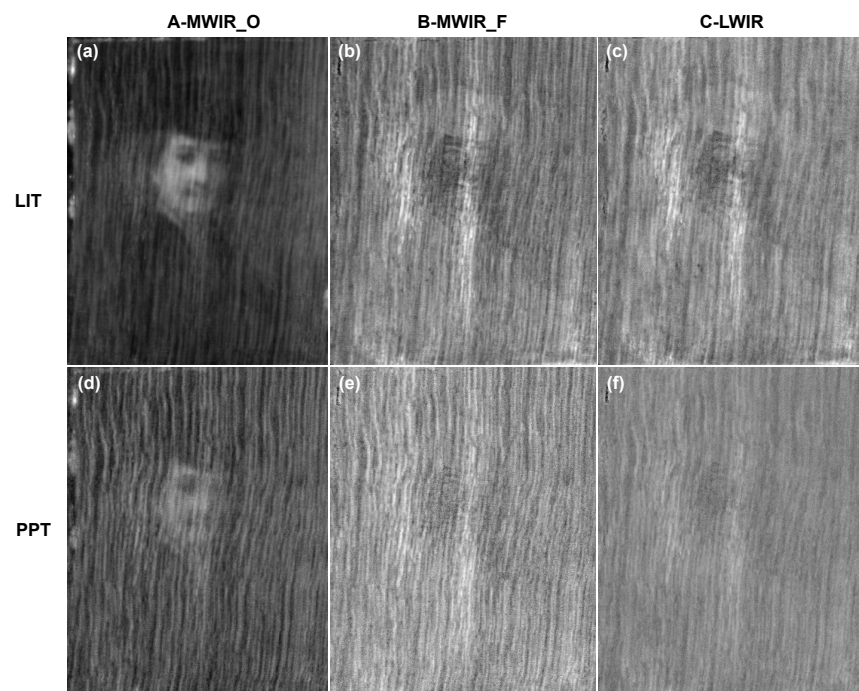
Figure 5. LIT and PPT phase images of the Rembrandt copy for all camera setups. The upper paint layers are almost entirely invisible and the structure of the wooden board is revealed. PPT phase images (**d**–**f**) show less of the paint layer when compared to LIT phase images (**a**–**c**). The wood grain contrast seems higher for the images obtained with the B-MWIR setup _F setup (**b**,**e**) when compared to the C-LWIR setup (**c**,**f**).
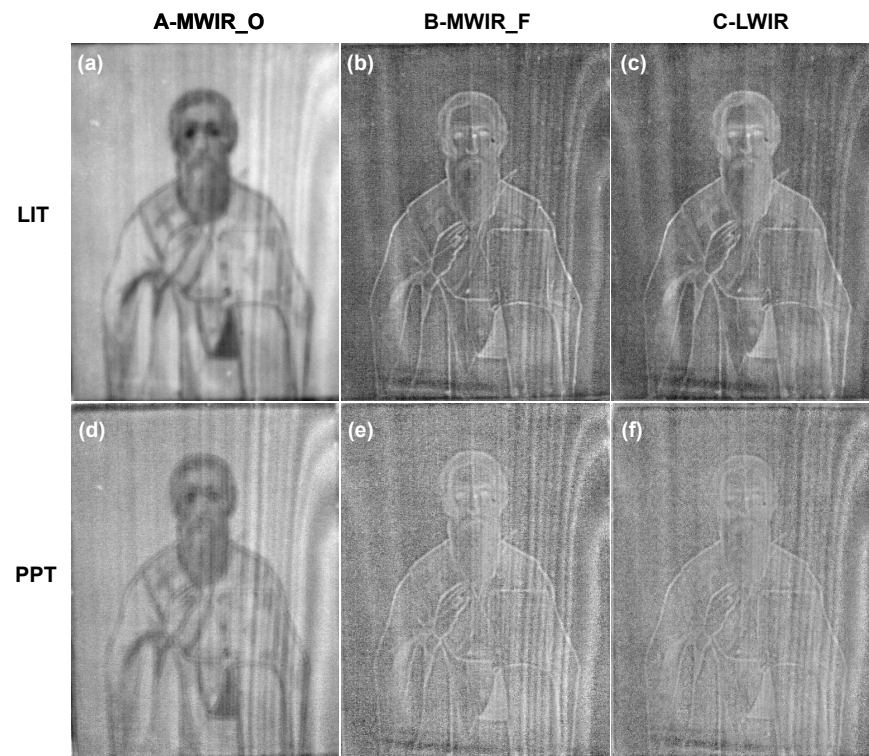
Figure 6. LIT and PPT phase images of the St. Nicholas icon for all camera setups. By eliminating the influence of the reflections, we can clearly visualize the pencil drawing (**b**,**c**,**e**,**f**). In the LIT phase images (**a**–**c**) the pencil drawing and smaller surface defects have a higher contrast, and the images appear less noisy overall, when compared to the PPT phase images (**d**–**f**).

As previously discussed, phase images are affected less by thermal and optical non-uniformities. This includes non-uniformities caused by the uneven heating of the upper paint layer, because the different paints absorb different amounts of illumination during thermal excitation [11]. As a result, the upper paint layer is also less visible, which is of particular interest when inspecting the wood grain of the support (Figure 7f). On the other hand, some of the surface defects are more pronounced in the amplitude images of the St. George painting (Figure 7a) and St. Nicholas icon (Figure 7b). This may be explained by the damaged areas absorbing and emitting radiation differently from the sound areas, which the amplitude images are more sensitive to. Appendix A, Figures A1–A3 contain all phase and amplitude images of each painting, for each method and camera setup.
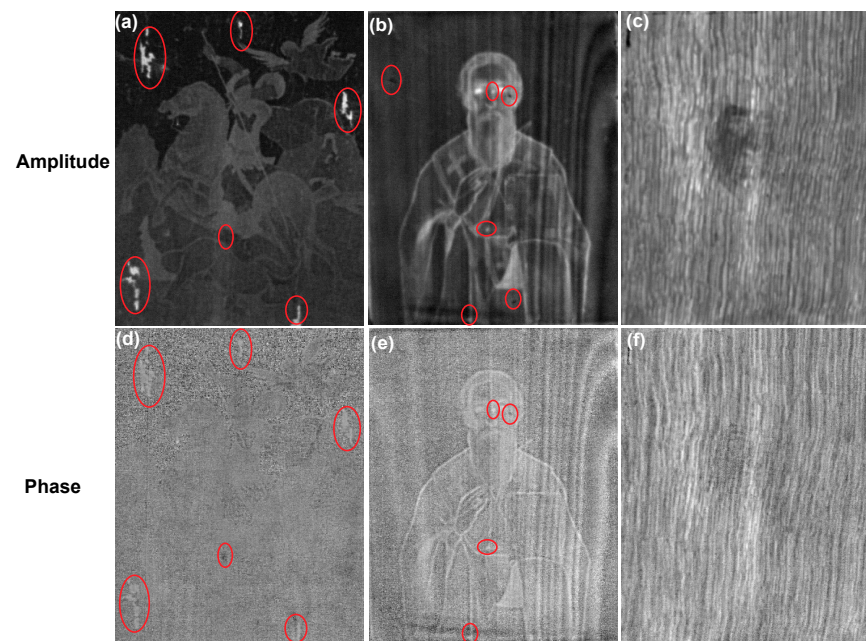
Figure 7. LIT amplitude and phase images of each painting for the B-MWIR_F setup. Some of the surface defects are more pronounced in the amplitude images (**a**,**b**) when compared to the phase images (**d**,**e**). Several defect areas are circled in red. Phase images (**f**) are influenced less by the upper paint layer than amplitude images (**c**).

4. Conclusions

We compared LIT and PPT techniques, and how their results are affected by the wavelength range of the used camera, with respect to qualitative inspections of paintings. For this purpose, three paintings of different natures were measured with different combinations of measurement techniques and camera setups. The measurement results are presented as a side-by-side comparison.

With two different thermal cameras, an MWIR and LWIR camera, three different camera setups were arranged, each with a different spectral range. It was shown that the camera setup in the 2.5–5 µm range suffers from direct reflection artifacts, caused by reflections from the halogen lamps. As discussed, these artifacts were most severe for the continuous illuminated LIT measurements, but were also observed in PPT measurements, due to the residual heat of the lamps. Restricting the wavelength range to >4.1 µm with a long-pass filter has effectively reduced the appearance of these artifacts. When combined with the long-pass filter, the images obtained with the MWIR camera looked very similar to those of the LWIR camera. An additional advantage of MWIR cameras is that they can be simultaneously used for IRR measurements. In this way, the same measurement setup can be used for both IRT and IRR measurements, while only having to swap out filters.

The NETD, or thermal contrast, of the cameras also appeared to have a noticeable impact on the processed results, with the camera setups with a lower NETD producing higher contrast images.

The maximum temperature fluctuation for the LIT measurements was 1.8 °C, compared to 2.7 °C for the PPT measurements. LIT and PPT measurements produce both phase and amplitude images. It has been shown that, in the phase images, the paint layers were nearly completely invisible, revealing the structure of the underlying wooden support. The upper paint layers were least visible in the PPT phase images. On the other hand, the pencil drawings were most clearly visible in the LIT phase images. Overall, LIT images appeared to have a higher contrast and appeared to be less noisy. Another attractive feature of LIT is its ability to tune the depth resolution based on the modulation frequency. This could potentially be useful when trying to determine the stratigraphy of multi-layered paintings, and is a possible avenue for future research.

Author Contributions: Conceptualization, M.H., S.V. and B.R.; methodology, M.H., S.V. and B.R.; software, M.H., B.R. and S.S.; validation, M.H.; formal analysis, M.H.; investigation, M.H.; resources, G.S., G.V.d.S. and K.J.; data curation, M.H.; writing—original draft preparation, M.H.; writing—review and editing, B.R., S.V., S.S., G.S., G.V.d.S. and K.J.; visualization, M.H.; supervision, G.S. and G.V.d.S.; project administration, M.H.; funding acquisition, G.S., G.V.d.S. and K.J. All authors have read and agreed to the published version of the manuscript.

Data Availability Statement: Data available on request. The data presented in this study are available on request from the corresponding author.

Conflicts of Interest: The authors declare no conflict of interest.

Abbreviations

The following abbreviations are used in this manuscript:

IRT	Infrared thermograpy
PT	Pulse thermography
LIT	Lock-in thermography
PCT	Principal component thermography
PLST	Partial least squares thermography
PPT	Pulse phase thermography
DAC	Differential Absolute Contrast
TSR	Thermal signal reconstruction
MWIR	Mid-wave infrared
LWIR	Long-wave infrared
MA-rFTIR	Macroscopic Fourier transform infrared scanning in reflection mode
NETD	Noise equivalent temperature difference
AFOV	angular field of view

Appendix A

This appendix contains an overview of all phase and amplitude images of each painting for each method and camera setup.
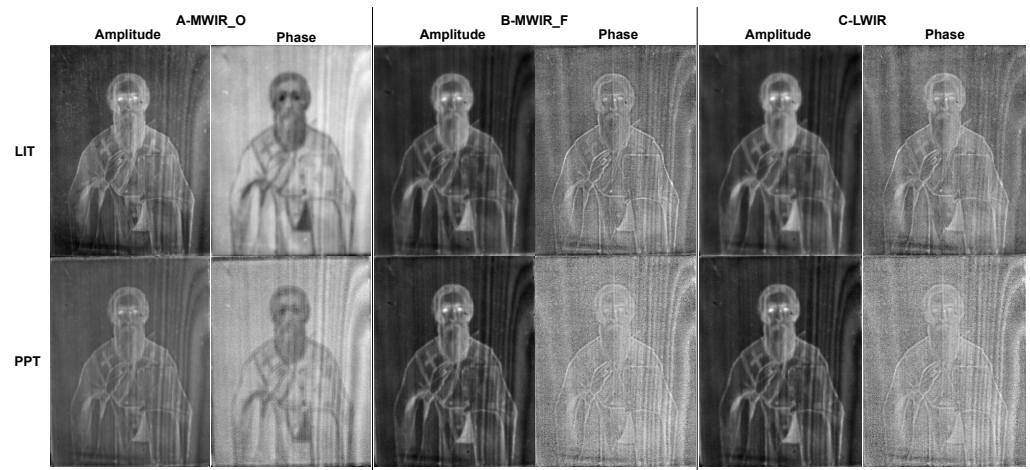
Figure A1. All measurement results for the icon, grouped by camera and technique.
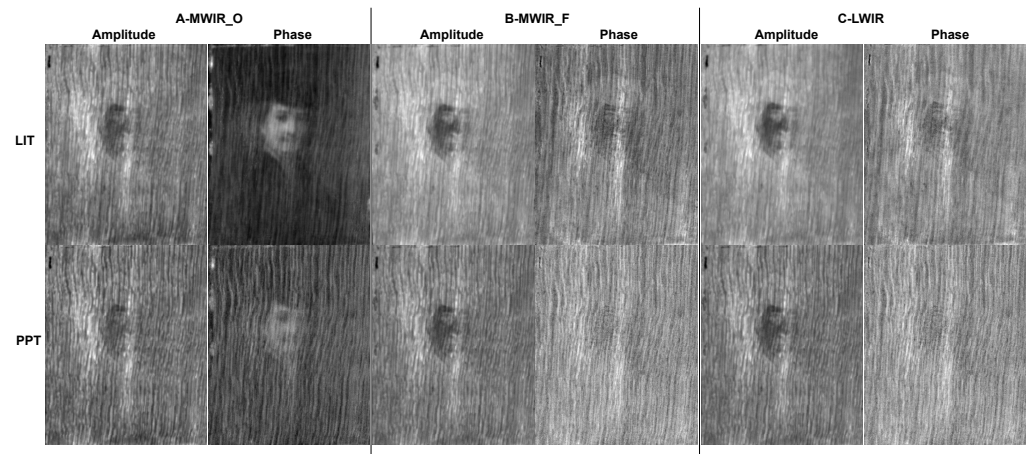

Figure A2. All measurement results for the portrait in the style of Rembrandt, grouped by camera and technique.
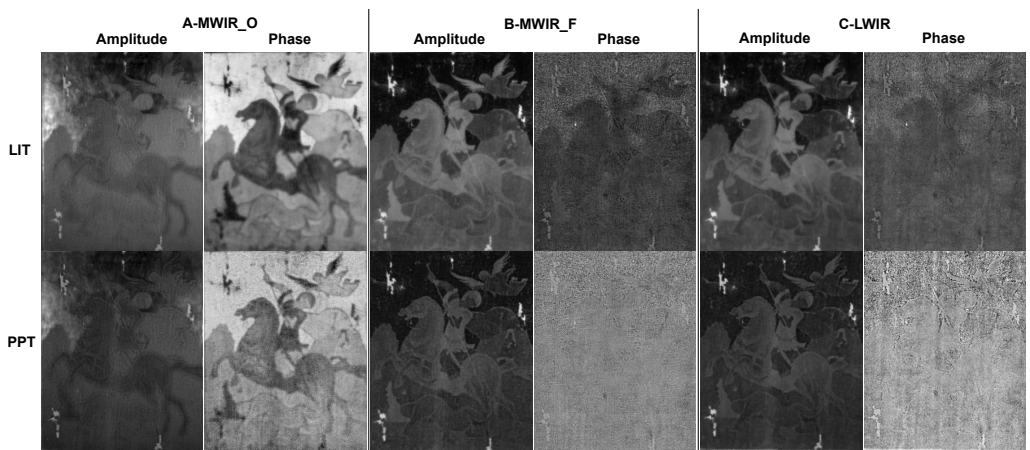

Figure A3. All measurement results for the St George painting, grouped by camera and technique.

References

1. Mercuri, F.; Orazi, N.; Paoloni, S.; Cicero, C.; Zammit, U. Pulsed thermography applied to the study of cultural heritage. *Appl. Sci.* **2017**, *7*, 1010. [CrossRef]
2. Laureti, S.; Sfarra, S.; Malekmohammadi, H.; Burrascano, P.; Hutchins, D.A.; Senni, L.; Silipigni, G.; Maldague, X.P.; Ricci, M. The use of pulse-compression thermography for detecting defects in paintings. *NDT E Int.* **2018**, *98*, 147–154. [CrossRef]
3. van der Snickt, G.; Dooley, K.A.; Sanyova, J.; Dubois, H.; Delaney, J.K.; Melanie Gifford, E.; Legrand, S.; Laquiere, N.; Janssens, K. Dual mode standoff imaging spectroscopy documents the painting process of the Lamb of God in the Ghent Altarpiece by J. And H. Van Eyck. *Sci. Adv.* **2020**, *6*, eabb3379. [CrossRef]
4. Rippa, M.; Pagliarulo, V.; Lanzillo, A.; Grilli, M.; Fatigati, G.; Rossi, P.; Cennamo, P.; Trojsi, G.; Ferraro, P.; Mormile, P. Active Thermography for Non-invasive Inspection of an Artwork on Poplar Panel: Novel Approach Using Principal Component Thermography and Absolute Thermal Contrast. *J. Nondestruct. Eval.* **2021**, *40*, 21. [CrossRef]
5. Gavrilov, D.; Maeva, E.; Grube, O.; Vodyanoy, I.; Maev, R. Experimental comparative study of the applicability of infrared techniques for non-destructive evaluation of paintings. *J. Am. Inst. Conserv.* **2013**, *52*, 48–60. [CrossRef]
6. Paoloni, S.; Mercuri, F.; Orazi, N.; Caruso, G.; Zammit, U. Photothermal approach for cultural heritage research. *J. Appl. Phys.* **2020**, *128*, 180904. [CrossRef]
7. Peeters, J.; Van der Snickt, G.; Sfarra, S.; Legrand, S.; Ibarra-Castanedo, C.; Janssens, K.; Steenackers, G. IR reflectography and active thermography on artworks: The added value of the 1.5–3 μm band. *Appl. Sci.* **2018**, *8*, 50. [CrossRef]
8. Zhang, H.; Sfarra, S.; Saluja, K.; Peeters, J.; Fleuret, J.; Duan, Y.; Fernandes, H.; Avdelidis, N.; Ibarra-Castanedo, C.; Maldague, X. Non-destructive Investigation of Paintings on Canvas by Continuous Wave Terahertz Imaging and Flash Thermography. *J. Nondestruct. Eval.* **2017**, *36*, 34. [CrossRef]
9. Maev, R.G.; Gavrilov, D. Thermography in Analysis of Works of Art: Choice of the Optimal Approach. In Proceedings of the 13th International Symposium on Nondestructive Characterization of Materials (NDCM-XIII), Le Mans, France, 20–24 May 2013. Available online: https://www.ndt.net/?id=15545 (accessed on 14 February 2023).
10. Ambrosini, D.; Daffara, C.; Di Biase, R.; Paoletti, D.; Pezzati, L.; Bellucci, R.; Bettini, F. Integrated reflectography and thermography for wooden paintings diagnostics. *J. Cult. Herit.* **2010**, *11*, 196–204. [CrossRef]
11. Mouhoubi, K.; Detalle, V.; Vallet, J.M. Improvement of the Non-Destructive Testing of Heritage Mural Paintings Using Stimulated Infrared Thermography and Frequency Image Processing. *J. Imaging* **2019**, *5*, 72. [CrossRef]
12. Blessley, K.; Young, C.; Nunn, J.; Coddington, J.; Shepard, S. The feasibility of flash thermography for the examination and conservation of works of Art. *Stud. Conserv.* **2010**, *55*, 107–120. [CrossRef]
13. Daffara, C.; Parisotto, S.; Ambrosini, D. Multipurpose , dual-mode imaging in the 3–5 μm range (MWIR) for artwork diagnostics: A systematic approach. *Opt. Lasers Eng.* **2018**, *104*, 266–273. [CrossRef]
14. Meola, C.; Carlomagno, G.M. Application of infrared thermography to adhesion science. *J. Adhes. Sci. Technol.* **2006**, *20*, 589–632. [CrossRef]
15. Candoré, J.C.; Bodnar, J.L.; Detalle, V.; Grossel, P. Non-destructive testing of works of art by stimulated infrared thermography. *EPJ Appl. Phys.* **2012**, *57*, 21002. [CrossRef]
16. Avdelidis, N.P.; Koui, M.; Ibarra-Castanedo, C.; Maldague, X. Thermographic studies of plastered mosaics. *Infrared Phys. Technol.* **2007**, *49*, 254–256. [CrossRef]
17. Sfarra, S.; Regi, M. Wavelet analysis applied to thermographic data for the detection of sub-superficial flaws in mosaics. *EPJ Appl. Phys.* **2016**, *74*, 31001. [CrossRef]
18. Fernandes, H.; Summa, J.; Daudre, J.; Rabe, U.; Fell, J.; Sfarra, S.; Gargiulo, G.; Herrmann, H.G. Characterization of ancient marquetry using different non-destructive testing techniques. *Appl. Sci.* **2021**, *11*, 7979. [CrossRef]
19. Chulkov, A.O.; Sfarra, S.; Saeed, N.; Peeters, J.; Ibarra-Castanedo, C.; Gargiulo, G.; Steenackers, G.; Maldague, X.P.; Omar, M.A.; Vavilov, V. Evaluating quality of marquetries by applying active IR thermography and advanced signal processing. *J. Therm. Anal. Calorim.* **2021**, *143*, 3835–3848. [CrossRef]
20. Mercuri, F.; Caruso, G.; Orazi, N.; Zammit, U.; Ceccarelli, S.; Cicero, C.; Vadrucci, M.; Paoloni, S. Depth-Resolved Analysis of Double-Layered Cultural Heritage Artifacts by Pulsed Thermography. *Int. J. Thermophys.* **2020**, *41*, 6. [CrossRef]
21. Palomar, T.; Agua, F.; Gómez-Heras, M. Comparative assessment of stained-glass windows materials by infrared thermography. *Int. J. Appl. Glas. Sci.* **2018**, *9*, 530–539. [CrossRef]
22. Hillen, M.; Legrand, S.; Dirkx, Y.; Janssens, K.; Van der Snickt, G.; Caen, J.; Steenackers, G. Cluster analysis of ir thermography data for differentiating glass types in historical leaded-glass windows. *Appl. Sci.* **2020**, *10*, 4255. [CrossRef]
23. Gavrilov, D.; Maev, R.G.; Almond, D.P. A review of imaging methods in analysis of works of art: Thermographic imaging method in art analysis. *Can. J. Phys.* **2014**, *92*, 341–364. [CrossRef]
24. Ceccarelli, S.; Guarneri, M.; Orazi, N.; Francucci, M.; Ciaffi, M.; Mercuri, F.; Paoloni, S.; de Collibus, M.F.; Zammit, U.; Petrucci, F. Remote and contactless infrared imaging techniques for stratigraphical investigations in paintings on canvas. *Appl. Phys. B Lasers Opt.* **2021**, *127*, 106. [CrossRef]
25. Sfarra, S.; Laureti, S.; Gargiulo, G.; Malekmohammadi, H.; Sangiovanni, M.A.; La Russa, M.; Burrascano, P.; Ricci, M. Low Thermal Conductivity Materials and Very Low Heat Power: A Demanding Challenge in the Detection of Flaws in Multi-Layer Wooden Cultural Heritage Objects Solved by Pulse-Compression Thermography Technique. *Appl. Sci.* **2020**, *10*, 4233. [CrossRef]

26. Legrand, S.; Alfeld, M.; Vanmeert, F.; De Nolf, W.; Janssens, K. Macroscopic Fourier transform infrared scanning in reflection mode (MA-rFTIR), a new tool for chemical imaging of cultural heritage artefacts in the mid-infrared range. *Analyst* **2014**, *139*, 2489–2498. [CrossRef] [PubMed]

27. Busse, G.; Wu, D.; Karpen, W. Thermal wave imaging with phase sensitive modulated thermography. *J. Appl. Phys.* **1992**, *71*, 3962–3965. [CrossRef]

28. Maldague, X.; Marinetti, S. Pulse phase infrared thermography. *J. Appl. Phys.* **1996**, *79*, 2694–2698. [CrossRef]

29. Schlangen, R.; Deslandes, H.; Lundquist, T.; Schmidt, C.; Altmann, F.; Yu, K.; Andreasyan, A.; Li, S. Dynamic lock-in thermography for operation mode-dependent thermally active fault localization. *Microelectron. Reliab.* **2010**, *50*, 1454–1458. [CrossRef]

30. Galmiche, F.; Leclerc, M.; Maldague, X.P. Time aliasing problem in pulsed- phased thermography. *Thermosense XXIII* **2001**, *4360*, 550–553. [CrossRef]

31. Maldague, X.; Galmiche, F.; Ziadi, A. Advances in pulsed phase thermography. *Infrared Phys. Technol.* **2002**, *43*, 175–181. [CrossRef]

32. Ibarra-Castanedo, C.; Maldague, X. Pulsed phase thermography reviewed. *Quant. Infrared Thermogr. J.* **2004**, *1*, 47–70. [CrossRef]

33. Pickering, S.G.; Chatterjee, K.; Almond, D.P.; Tuli, S. LED optical excitation for the long pulse and lock-in thermographic techniques. *NDT E Int.* **2013**, *58*, 72–77. [CrossRef]

34. Pickering, S.; Almond, D. Matched excitation energy comparison of the pulse and lock-in thermography NDE techniques. *NDT E Int.* **2008**, *41*, 501–509. [CrossRef]